Proceedings of IPACK2007
ASME InterPACK '07
July 8-12, 2007, Vancouver, British Columbia, CANADA

IPACK2007-33829

DESIGN OPTIMIZATION OF FIXED-VALVE MICROPUMPS FOR MINIATURE COOLING SYSTEMS

Fred K. Forster
Travis Walter
Department of Mechanical Engineering
University of Washington
Seattle Washington 98195
Email: forster@u.washington.edu

ABSTRACT

The piezoelectrically driven fixed-valve micropump may be an attractive choice for miniature liquid cooling systems due to its low-cost potential and simple fabrication. The thin, stackable design can be fabricated in many materials, including silicon, metal and plastic. Previous linear system modeling has been used to predict resonant behavior in terms of valve Reynolds number and used as a guideline for design, but can not yield predictions of pressure and flow, which depend on nonlinear fluid dynamic phenomena. In this study we report an extended model that incorporates the calculation of block-load pressure and no-load flow in a manner such that thousands of designs can be analyzed quickly. The results indicate that by calculating these two pump performance parameters over a design space of valve size and actuator stiffness, pump design is better able to match pump performance to system requirements. Experimental verification was performed using prototype pumps with interchangeable plastic and metal parts to demonstrate the approach for these two low cost materials.

NOMENCLATURE

AR valve channel aspect ratio d_v/w_v
C fluid compliance (m^3/Pa)
d diodicity functional in Eq. (2)
d_v valve channel depth (m)
D_h valve hydraulic diameter $2w_v/(1+1/AR)$ (m)
Di valve diodicity
E_{depol} depoling voltage gradient nominally $5\times10^5\,\mathrm{V/m}$
f circular frequency (Hz)
I fluid inertance ($\mathrm{Pa\,s}^2/\mathrm{m}^3$)
L_f shortest centerline path length through valve (m)
P_{atm} ambient atmospheric pressure (Pa)
P_{bl} pump mean block-load (no flow) pressure (Pa)
$p_c(t)$ pump chamber pressure, also $p_s(t)$ (Pa)
P_{cm} pump mean chamber pressure (Pa)
$p_l(t)$ pump load (back) pressure (Pa)
$p_s(t)$ source (chamber) pressure in Fig. 3, also $p_c(t)$ (Pa)
$q(t)$ volume flow rate (m^3/s)
Q_{nl} pump no-load net volume flow rate (m^3/s)
Q_s source (chamber) volume flow rate harmonic amplitude delivered to both valves in Fig. 3 (m^3/s 0-to-pk)
Q_v volume flow rate harmonic amplitude through one valve approximated by a straight channel (m^3/s 0-to-pk)
Re valve Reynolds number based on hydraulic diameter $2q_v/(d_v+w_v)\nu$
R fluid resistance ($\mathrm{Pa\,s/m}^3$)
t^* nondimensional time ft
t_p pump chamber cover plate thickness (m)
V_s supply voltage harmonic amplitude (V 0-to-pk)
w_v valve channel width in Fig. 1 (m)
ν kinematic viscosity (m^2/s)
$(\,)_i$ inlet valve
$(\,)_o$ outlet valve
$(\,)_t$ cylindrical inlet/outlet ports
$(\,)_v$ property of both inlet and outlet valves

INTRODUCTION

The concept of a fixed-geometry valve goes back to at least the early part of the 20th century to control the flow of gas [1] and more recently in liquid applications [2]. Such macroscopic uses involve high Reynolds number flows that would be expected

to behave substantially different in small-scale devices. A mesoscopic liquid diaphragm pump was reported in the MEMS community about 15 years ago [3], which showed additional promise for fixed valves. However, it was also a fairly high Reynolds number device [4]. Shortly thereafter, a number of microfabricated diaphram pumps appeared in the literature [5–7]. Since the 1980s, however, many other designs of micropumps have been reported, including other types of reciprocating displacement pumps and electroosmotic, electrohydrodynamic and magnetohydrodynamic designs [8]. What remains of significant interest in the case of the fixed-valve pump is its simplicity, ability to work with particlulate flows and low potential costs of materials and fabrication. But much of the development has been based on empirical methods, which has been a deterrent to its wide-spread use.

Currently we are developing improved design techniques for fixed-valve pumps with applications to electronic cooling. By the time of this study we have developed optimization techniques for circular piezoelectric bimorph actuators that yield maximum volume displacement per volt by optimizing the diameter and thickness of the piezoelectric element and the thickness of the elastic cover plate, to which the piezoelectric element is attached, for a given cover plate diameter, i.e. pump chamber diameter, and material [9]. We have also developed a linear reduced-order (lumped-parameter) system model that has been demonstrated to accurately model all aspects of pump geometry and materials except for the nonlinear fluid dynamic behavior in the valves by accurate predictions of system response when straight rectangular channels replace the fixed-geometry valves [10, 11]. Lastly, we have studied valve geometrical shape and developed an optimized version of the Tesla-type valve [12–14]. With this knowledge we have developed two different pumping systems with the ability to move approximately 40W of thermal energy from a $2.5\,\mathrm{cm}^2$ surface [15, 16]. In the study reported here we have added non-linear fluid dynamic behavior of the valves to the existing linear system model [10] and performed an experimental investigation to evaluate this extended model. This work shows how valve size and cover plate stiffness leads to significantly different pump pressure-flow relationships. With this information a pump can be designed to generate higher block load pressure, usually at the cost of lower no-load flow, or vice versa, i.e. modify the basic pump characteristics to rationally design a pump to meet particular system requirements with the starting point being only pump chamber diameter and cover plate material.

METHODS

Existing Model

The starting point for the current model is the linear systems model previously described [10] and only briefly presented here. It is composed of lumped parameters to characterize the piezoelectric actuator, compliance and flow resistance and inertance of the fluid in the pump chamber, resistance and inertance of the fluid in the valves and compliance, resistance and inertance as seen from the entrance and exit of the pump [10, Fig. 3].

The actuator is characterized by its stiffness k, effective mass m, centerline displacement per volt f_e and a shape factor γ, which is the ratio of the displaced volume of the inner surface of the piezoelectric/cover plate to that displaced by a piston having the same centerline displacement. These quantities are determined by the thickness and diameter of the piezoelectric element that yields maximum volume displacement per volt for a given material and cover plate (pump chamber) diameter. This is done using finite element analysis (FEA).

The fluid inertance and resistance of the working fluid in the pump chamber are relatively unimportant except for exceedingly shallow pump chambers, but the compliance includes the important contribution of an effective quantity of gas. Two other contributors to compliance are the pump housing (calculated with FEA) and the compliance of the working liquid. The model is capable of handling gas or liquid working fluids, although only liquid is of interest in this study.

The resistance and inertance of the valves is based on an equivalent straight length rectangular duct and the exact solution of the Navier-Stokes equation for fully developed oscillatory laminar flow. Since Tesla-type valves were used in this study, the cross sectional width w_v and depth d_v of the equivalent duct are those of the valve, and the equivalent length L_f is length of the shortest (forward flow) centerline path through the valve, which is a slight departure from previous work. These assumptions are discussed in detail elsewhere [10].

The compliance, resistance and inertance of the connected tubes have, by design, only a small effect on performance due to the size and distensibility of the tubing. Their purpose is to capacitively decouple the pump from the rest of the flow system. Otherwise, performance is greatly affected by high frequency flow oscillations that would be transmitted to all points up and downstream from the pump.

The maximum excitation voltage considered, which defines the maximum system output, is determined by the lowest of power supply limit, depolarization limit of the piezoelectric element, which is a function of its thickness and material properties, and cavitation voltage. Cavitation is modeled to occur when the minimum absolute chamber pressure, which occurs during the filling phase, equals the vapor pressure of the working fluid at ambient temperature. This is a simplified cavitation criterion that does not take into account lower pressure in the valves due to increased velocity [14].

A typical use of the model as described above is the consideration of a design space of valve size and cover plate thickness and from a surface plot of any desired output variable, infer pump characteristics. For example, a plot of the harmonic amplitude of Reynolds number Re in the valves might imply good net flow and pressure since the directional behavior of the valves, described by diodicity Di, the ratio of pressure drop in the reverse to forward direction, would be expected to increase with increasing Re. Typical output quantities considered in addition to Re are harmonic amplitudes of valve volume flow rate Q_v, chamber pressure P_c and actuator centerline velocity V_m.

Model Extension

For this study the departure from the current model described above was a more detailed description of the valve. In addition to the cross-sectional dimensions and equivalent length, the nonlinear directional behavior described in terms of diodicity Di was included. That behavior was assumed to be characterized by steady-state, two-dimensional flow characteristics. For a given shape and based on dimensional analysis this can be summarized by a single curve of Di versus Re valid for any size valve assuming laminar flow, which is usually valid for the small valves associated with pumps of interest. Our previous work considered both the diffuser and Tesla-type valve and optimized the geometry of each with steepest decent methods using computational fluid dynamics (CFD) [13]. On the basis of that study the optimized Tesla-type valve given in Figure 1 was used over the optimized diffuser valve.

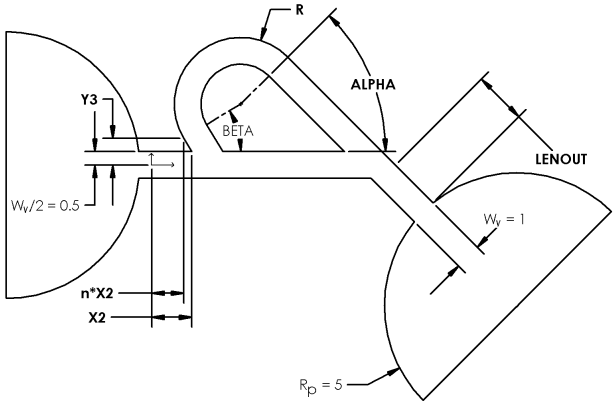

Figure 1. THE SIX PARAMETERS THAT DEFINE THE SHAPE OF THE OPTIMUM TESLA-TYPE VALVE ARE 1) $X2 = 1.60$ THE LENGTH OF THE INLET (LEFT) CHANNEL IN FORWARD FLOW, 2) $Y3 = 0.608$, 3) SCALE FACTOR $n = 0.79645$, SUCH THAT $(nX2, Y3)$ DEFINES A TERMINAL TANGENT SEGMENT OF THE LOOP, 4) LOOP OUTER RADIUS $R = 2.35$, 5) OUTLET CHANNEL LENGTH $LENOUT = 2.94$,, BASED ON THE INTERSECTION OF THE UPPER EDGE OF THE OUTLET CHANNEL AND THE x-AXIS, AND 6) OUTLET CHANNEL ORIENTATION ANGLE $\alpha = 41.9^\circ$. THE RETURN ANGLE $\beta = 71.7^\circ$ IS DETERMINED BY $X2, Y3$ AND n. THE COORDINATE SYSTEM SHOWN IS LOCATED ON THE CENTERLINE OF THE INLET CHANNEL ONE-HALF CHANNEL WIDTH TO THE RIGHT OF THE PLENUM/CHANNEL INTERSECTION. ALL DIMENSIONS ARE NORMALIZED BY CHANNEL WIDTH w_v. THE SEMICIRCULAR PLENUMS OF RADIUS $R_P = 5$ MODEL PUMP CHAMBER AND PLENUMS FOR CFD CALCULATIONS TO INCLUDE INLET AND EXIT FLOW LOSSES. THESE VALUES ARE FROM [14]. IN ADDITION, THE NORMALIZED VALVE LENGTH ALONG THE CENTERLINE FOR FORWARD FLOW $L_f/w_v = 10.8$.

For the optimal valve geometrical parameters given in Fig. 1 and shown in Fig. 2, the net pressure and flow were determined by numerical solution of simple nonlinear ordinary differential equations based on a low-order model of the flow through the pump for the harmonic amplitude of volume flow rate generated in the pump chamber and available to both valves approximated by $2Q_v$ from the linear model. There are a number of ways that the governing equations can be formulated with the associated trade-off between computational effort and accuracy. Two possible ways are based on calculated diodicity Di versus Re or non-dimensional pressure drop in each flow direction versus Re, which like Di versus Re, describes the behavior of the same shaped valve for any size. But to demonstrate the simplest approach, a constant value of Di was utilized in this study equal to the that at the rms level of valve volume flow rate $Q_v/\sqrt{2}$ or equivalently the rms level of Re.

Net no-load volume flow rate Q_{nl} was calculated based on the circuit shown in Fig. 3. The input volume flow rate available to the parallel arrangement of inlet and outlet valves and tubes is given by $q_s(t) = Q_s \sin 2\pi ft$, where $Q_s = 2Q_v$ as described above. The pressure drop loop equation is given by

$$I\frac{dq_o}{dt} + R_o q_o + I\frac{dqi}{dt} + R_i q_i = 0 \tag{1}$$

where $I = I_v + I_t$ is the sum of inertances of each valve and each connecting tube assuming inlet and outlet are identical. Each was calculated according to analytical solutions of the Navier-Stokes equation for fully-developed harmonic flow at the driving pump frequency f in straight ducts of rectangular and circular cross section, respectively. Also, $R_o = R_v d_o + R_t$, and $R_i = R_v d_i + R_t$, where R_v and R_t were also calculated from the Navier-Stokes equations, and the nonlinearity of the valve resistance was described by d_o and d_i, where

$$d_o = \begin{cases} 1 & \text{if } q_o \geq 0 \\ \mathrm{Di}(|q_o|) & \text{otherwise} \end{cases} \text{ and } d_i = \begin{cases} 1 & \text{if } q_i \geq 0 \\ \mathrm{Di}(|q_i|) & \text{otherwise} \end{cases} \tag{2}$$

The definitions of d_o and d_i were chosen to reflect the assumption that forward flow in a Tesla-type valve is unaffected by the loop and approximated by flow in a straight rectangular duct of length L_f. This is suggested, for example, in a typical calculated velocity magnitude field shown in Fig. 2. Noting $q_i = q_o - q_s$ and introducing non-dimensional time $t^* = ft$, the final form of the equation used to calculate no-load flow is given by

$$\frac{dq_o}{dt^*} = \frac{R_o + R_i}{2fI} q_o + Q_s \left(\pi \cos 2\pi t^* - \frac{R_i}{2fI} \sin 2\pi t^* \right) \tag{3}$$

This equation was solved with an explicit Runge-Kutta, Dormand-Prince pair formula needing only the immediately preceding time point using Matlab v6.5 (The Mathworks). The net no-load flow was then calculated after the simulation reached steady-state, at which point the average of the time series was calculated to yield Q_{nl}.

Net block-load pressure P_{bl} was determined in a similar manner. The governing equation was also based on Fig. 3 with

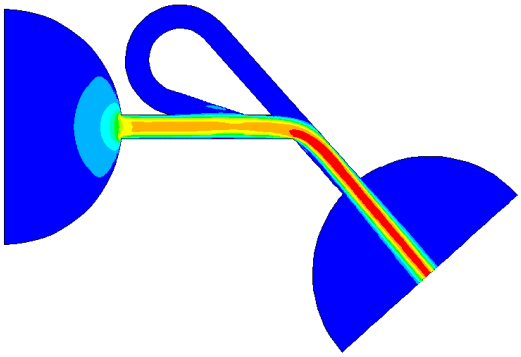

(a) FORWARD FLOW

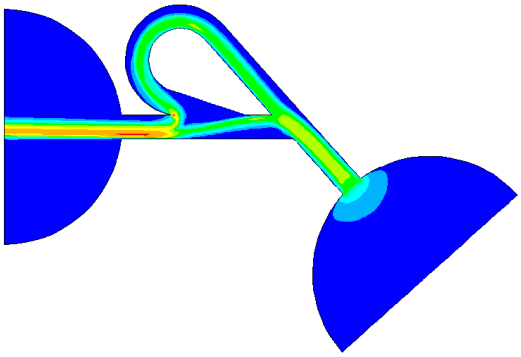

(b) REVERSE FLOW

Figure 2. OPTIMUM SHAPE TESLA-TYPE VALVE FOR PARAMETERS GIVEN IN FIG. 1. SIX-LEVEL CONTOUR PLOT CORRESPONDS TO STEADY TWO-DIMENSIONAL FLOW VELOCITY MAGNITUDE FOR TYPICAL VALUES OF VALVE RMS REYNOLDS NUMBER [17].

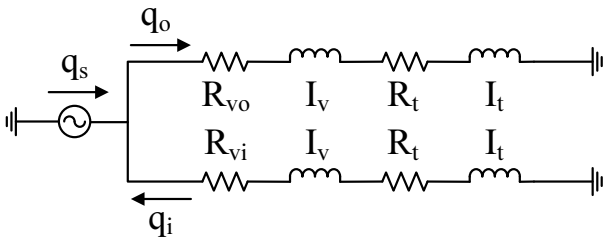

Figure 3. SCHEMATIC PUMP CIRCUIT USED TO CALCULATE NO-LOAD FLOW RATE.

the addition of a capacitor C between the outlet tube inertance and ground. This yields Eq. (1) again but with a the term for the pressure drop p_l across the load capacitor added to the left side. Noting $q_o = C dp_l/dt$ and following the same procedure described above, the governing equation is given by

$$\frac{d^2 p_l}{dt^{*2}} = -\frac{R_o + R_i}{2fI}\frac{dp_l}{dt^*} - \frac{1}{2Cf^2 I}p_l + \frac{Q_s}{Cf}\left(\frac{R_i}{2fI}\sin 2\pi t^* + \pi \cos 2\pi t^*\right) \quad (4)$$

The mean load pressure in steady state is not a function of C and was set to $I/(R_v + R_t)^2$, which allowed steady state to be reached in a reasonable time, after which integration was performed to obtain P_{bl}. Since the linear model considers the onset of cavitation to determine the maximum input voltage as discussed above, p_s was also calculated. It is pressure drop across the entire outlet branch,

$$p_s = p_c = R_o q_o + fI\frac{dq_o}{dt^*} + p_l \quad (5)$$

where $q_o = fC dp_l/dt^*$ was directly available from the numerical solution and numerically differentiated to obtain dq_o/dt^*. The mean chamber pressure P_{cm} was then determined by integration. An iterative loop was performed within the linear model with the absolute chamber pressure $P_{atm} + P_{cm}$ updated at each step.

Experiments

The pumps used for testing consisted of three basic parts, an acrylic block in which the pump chamber and valves were machined, a brass cover plate, on which a lead-zirconate-titanate (PZT) piezoelectric disk was attached to form the actuator, and a second acrylic block with a circular recess to give the membrane room to move after the plate was sandwiched between the blocks. Geometry for machining was generated with FeatureCAM v8 (Engineering Geometry Systems), and machining performed on a CNC mill (Bridgeport model V2XT) with a standard 1/8 inch collet that held 2-flute (127, 254 and 508 μm (0.005, 0.01 and 0.02 in)) carbide end mills (Richard MicroTool). A hole was also drilled through the center of the recess in the latter block to allow for laser vibrometer measurements in addition to holes in each block for two alignment pins and holes needed to connect inlet/outlet tubes to the chamber block. The piezoelectric disks (Piezo Systems PZT-5A) were milled from stock to obtain the desired diameter, then fastened to the brass cover plate with silver epoxy (Epoxy Technologies type H31). Then a small piece of bead tape was affixed to the center of the PZT for vibrometer measurements. Stainless steel inlet/outlet tubes having a 2.08 mm inner diameter and 10 mm long were bonded to each chamber block with a quick-set epoxy, and attached to them were 5 mm inner diameter PVC tubes that ran to the inlet reservoir and pressure transducer or small beaker depending on the particular test done.

Assembly of the pumps consisted of applying a silicone grease to the parts and clamping them together with alignment pins in place. Each assembled pump was filled with mineral spirits and left for one hour to dissolve any remnants of grease in the valves and then flushed with isopropyl alcohol followed by deionized water. Figure 4 shows an assembled pump. Other parts that make up an assembled pump seen in the photograph are an electrical connector to the PZT element and a block to facilitate clamping the assembly together. Three valve sizes and brass cover plate thicknesses were utilized, allowing for a total of nine different micropumps to be assembled.

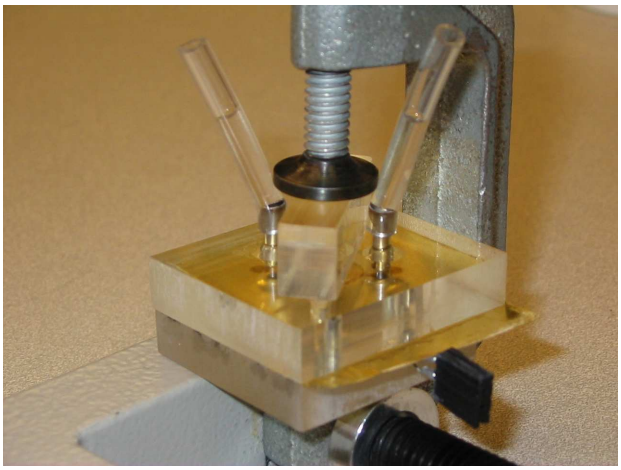

Figure 4. ASSEMBLED MICROPUMP CONSISTING OF A CLAMP SPACER BLOCK, A TOP BLOCK CONTAINING CHAMBER, VALVES AND INLET/OUTLET TUBES, A COVER PLATE AND ATTACHED PZT DISK AND A BOTTOM BLOCK WITH A RECESS FOR ACTUATOR DISPLACEMENT AND HOLE FOR LASER VIBROMETER MEASUREMENTS OF ACTUATOR VELOCITY.

The experimental procedures for each pump consisted of measuring the resonant frequency of the actuator for each assembled pump before it was filled with water using a laser vibrometer (Polytec model OVF 302) and noting the frequency at which the centerline velocity was maximum. Although this frequency was well above the liquid-filled resonant frequency, it was used to determine if there were any major electrical problems or problems with bonding or cracking of the piezoelectric element. Pumps were then filled with water degassed by boiling after first flushing with degassed isopropyl alcohol, which more easily wetted the valves and chamber. Block-load pressure and no-load flow were measured by driving the pumps with an sinusoidal signal (Wavetek model 19)that was further amplified (Piezo Systems Linear Amplifier).

Block-load pressure was measured with a pressure transducer (Honeywell type 142PC30D) with the pump mounted such that the inlet/outlet tubes were horizontal and at the same height as the inlet reservoir and the water/air interface in the outlet tube attached to the pressure transducer. No-load flow was measured by removing the pressure transducer and measuring the weight of water pumped over a significantly long time to minimize errors.

RESULTS AND DISCUSSION

Pumps with footprint of about an inch square have been our primary interest since that appears to be a reasonable size for use in electronic cooling of small systems and heat removal on the order of 100W. We have worked with that size previously [15, 16]. Thus, the starting point for pump design was a 10 mm diameter pump chamber. A plastic pump body was chosen to investigate the use of a very low cost material. Brass for the cover plate was chosen because a wide variety of thicknesses were readily available. Except for physical properties of the materials utilized including fluids, no other empirical data were used for the design analysis. Since the pump is a resonant device, some parameters were more important than others. One of two critical parameters was valve cross-sectional size since its contribution to inertial and dissipative characteristics of the overall system were highly significant. The other critical parameter was actuator stiffness. Even so, one compromise made for this study was consideration of only one combination of PZT diameter and thickness (9 mm and 127 μm), even though the design approach can include optimization of both parameters. To further simplify the study, and based on limitations of the machining methods, all valves had an aspect ratio $AR = 2.5$ with chamber depth equal to the valve depth. Given that the effects of valve size and actuator stiffness are quite significant compared to the effects of the parameters held constant, this study was considered an investigation of design optimization methods for a particular diameter pump.

Figure 5 shows the design space of valve width and cover plate thickness over which the harmonic amplitude of valve Reynolds number was calculated using the existing linear model. A main characteristic of the surface shown is that the region of higher values corresponds to a ridge parallel to each axis. Since diodicity is higher at higher Re, one might expect good pump performance over a range of valve width for thin cover plates or to a lesser extent for a range of cover plate thickness for smaller valves. Figure 6 and Fig. 7 show new results based on the nonlinear model implemented in this study for no-load flow Q_{nl} and block-load pressure P_{bl} over the same design space. Higher values of each fall into regions of higher Reynolds number shown in Fig. 5. However, the two regions overlap but do not coincide. There is clearly a trade-off between these two performance characteristics. Figure 8 shows the range of calculated performance characteristics at each grid point of the entire design space considered. This figure shows that not only are there combinations of higher flow-lower pressure and vice versa, but many intermediate combinations. This suggests that within an overall range of pressure and flow a pump can be designed to have any number of pressure-flow attributes by simply modifying valve size and cover plate thickness.

To compare these findings with experiment, choices were made that resulted in chamber blocks and actuators assemblies shown in Tabs. 1 and 2. A point in the design space $[t_p, w_v] = [102, 300]\,\mu$m was chosen as a nominal combination of cover

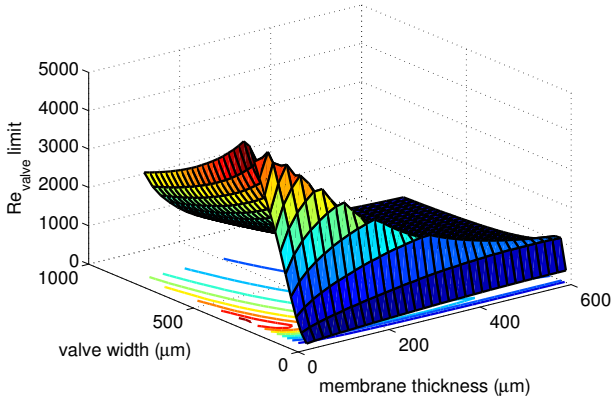

Figure 5. LINEAR MODELING RESULTS SHOWING THE HARMONIC AMPLITUDE OF VALVE REYNOLDS NUMBER FOR A 10 mm DIAMETER PUMP WITH A BRASS COVER PLATE, PZT THICKNESS OF 127 μm (DEPOLING ELECTRIC FIELD $E_{depol} = 5 \times 10^5$) AND DIAMETER OF 9 mm, WORKING FLUID WATER WHOSE PROPERTIES (INCLUDING VAPOR PRESSURE) CORRESPOND TO 25 °C AND DRIVEN AT A SUPPLY VOLTAGE AMPLITUDE $V_s = 64$ V 0-TO-PK. VALVE ASPECT RATIO $AR = 2.5$

plate thickness and valve size. Two more values for each coordinate above and below the nominal, were also chosen, which gave a matrix of nine pump configurations to test. Figure 9 shows the subset of calculated performance characteristics for the fabricated pumps, which covers a reasonable portion of the more complete design space shown in Fig. 8.

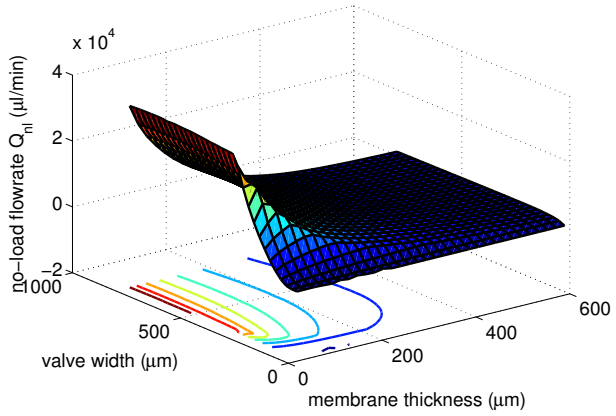

Figure 6. NON-LINEAR MODELING RESULTS SHOWING NO-LOAD FLOW FOR THE SAME PARAMETERS GIVEN IN FIG. 5.

Table 3 shows the resonant frequency of empty and liquid filled pumps. Only membrane M04 showed a deviation from that calculated of more that 5%. However, good experimental repeatability for that membrane indicated that integrity between the PZT disk and cover plate was good, and that the difference

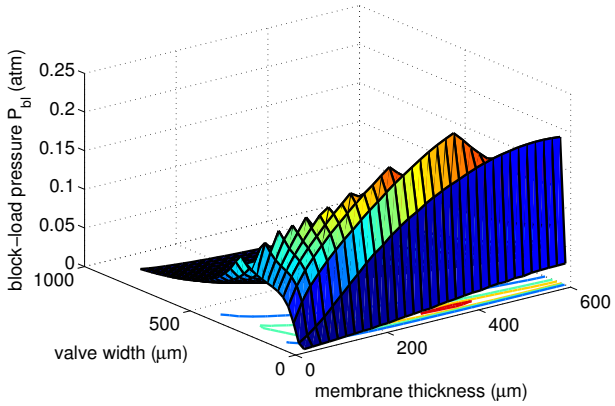

Figure 7. NON-LINEAR MODELING RESULTS SHOWING BLOCK-LOAD PRESSURE FOR THE SAME PARAMETERS GIVEN IN FIG. 5.

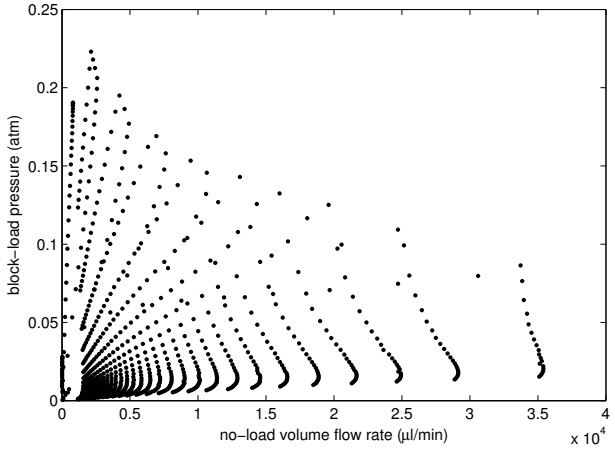

Figure 8. CALCULATED PUMP PERFORMANCE IN TERMS OF BLOCK-LOAD PRESSURE VERSUS NO-LOAD FLOW AT ALL GRID POINTS OF THE ENTIRE DESIGN SPACE AND FOR THE SAME PARAMETERS GIVEN IN FIG. 5.

Table 1. PROPERTIES OF CHAMBER BLOCKS USED TO FABRICATE PUMPS.

chamber block	valve width (μm)	chamber diameter (mm)	chamber & valve depth (μm)	valve aspect ratio
C01	300	10	750	2.5
C02	150	10	375	2.5
C03	600	10	1500	2.5

might have been caused by, for example, the amount of epoxy used to bond the PZT to the cover plate. Table 3 also provides

Table 2. PROPERTIES OF THE ACTUATOR ASSEMBLIES USED TO FABRICATE PUMPS.

actuator assembly	cover plate thickness (μm)	PZT thickness (μm)	PZT diameter mm
M02	76.2	127	9
M03	177.8	127	9
M04	101.6	127	9

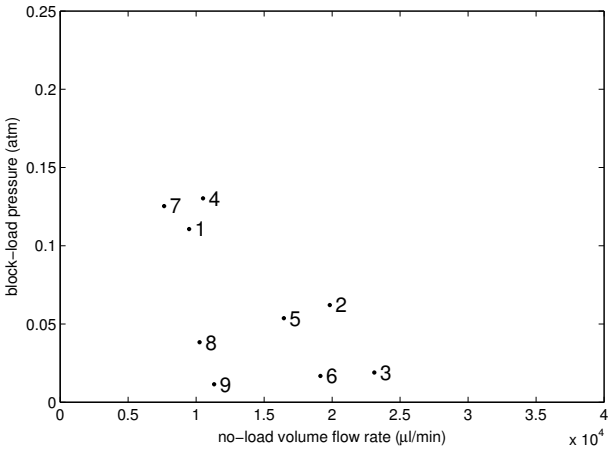

Figure 9. CALCULATED PUMP PERFORMANCE IN TERMS OF BLOCK-LOAD PRESSURE VERSUS NO-LOAD FLOW FOR THE NINE FABRICATED PUMPS FOR THE SAME PARAMETERS GIVEN IN FIG. 5. THE NUMBERS SHOWN CORRESPOND TO PUMP NUMBER IN TAB. 3.

Table 3. MEASURED AND CALCULATED PUMP RESONANT FREQUENCIES WITH DIFFERENCES IN CALCULATED RELATIVE TO MEASURED VALUES FOR APPLIED VOLTAGES THAT ARE SMALL COMPARED TO NORMAL OPERATING VOLTAGES. PUMP NAMES P1 TO P9 ARE IDENTIFIED THROUGH THE NOTATION Cmx,Mny, WHERE Cm and Mn REFER TO CHAMBER MEMBRANE TYPES NUMBERED m AND n AS DESCRIBED IN TABLES 1 AND 2. LETTERS x AND y IDENTIFY SPECIFIC CHAMBERS AND MEMBRANES FABRICATED. NOTE THE SAME CHAMBER AND MEMBRANE WAS USED FOR THE FABRICATION AND TESTING OF ALL NINE PUMPS.

pump	air			water		
	meas kHz	calc kHz	diff %	meas Hz	calc Hz	diff %
P1 (C02c,M02a)	9.0	9.0	0	341	348	2
P2 (C01f,M02a)	8.9	9.0	1	401	495	23
P3 (C03b,M02a)	8.6	9.0	5	418	411	-2
P4 (C02c,M04b)	11.6	10.0	-14	492	410	-17
P5 (C01f,M04b)	11.5	10.0	-13	554	583	5
P6 (C03b,M04b)	11.3	10.0	-12	593	776	31
P7 (C02c,M03e)	13.3	13.2	-1	613	630	3
P8 (C01f,M03e)	13.5	13.2	-2	708	884	25
P9 (C03b,M03e)	13.3	13.2	-1	1570	1160	-26

a similar comparison for the liquid-filled pump that ensured the filling process was successful and, for example, air had not entered the pump, which has a large effect on performance. Previous work indicates variations on the order of 20% are to be expected mainly due to the fact that valves are assumed to be straight rectangular ducts of length L_f [10].

Table 4 shows the measured and calculated values of block-load pressure and no-load flow for all nine fabricated pumps. The primary results correspond to an excitation of 64 V, and both measured and calculated values exist for all pumps at this voltage. Other voltage levels above and below 64 V are included to further investigate the primary results. The model over-predicted P_{bl} by factors of two to six and Q_{nl} by factors from five to eleven in columns one and two (pumps in column three produced no output at 64 V). These large differences were apparently due to neglecting entry and exit flow energy losses in the valve resistance calculations even though they were included in the calculated values of Di versus Re taken from [14]. This resulted in over-estimates of Q_s available to the valves due to less calculated system damping. In addition, since the calculations of P_{bl} and Q_{nl} are nonlinear, the effect of measured membrane motion being lower than that calculated may have further magnified these differences.

At higher voltage, another phenomenon appeared to affect the measured value of P_{bl} for most of the pumps in columns one and two. When the primary voltage was doubled to 125 V, measured P_{bl} increased by a factor of approximately three to seven. To compare these results to model calculations E_{depol} was doubled along with the increased voltage such that the output would only be limited by cavitation or supply voltage to reflect the experimental conditions at the higher voltage. The calculated values agreed more closely with the measured values. In the case of the nominal pump P5, the measured value was even higher than calculated. The reason for these results is apparently due to the cavitation occurring in the model before 125 V was reached, but not in the experiments. It can be seen in Tab. 4 that except for pumps P1 and P2, cavitation was reached before 125 V as evidenced by the plateauing of P_{bl}. While cavitation is always expected if a pump is driven at high enough voltage and the PZT does not depol, it apparently did not occur in any of the experiments before 125 V. Pump P7 is an example of what might be expected if an experimental pump cavitated. In that case it is possible that maximum P_{bl} was reached at the point of cavitation for both model and experiment, but cavitation for the model

Table 4. PUMP PERFORMANCE IN TERMS OF BLOCK-LOAD PRESSURE $P_b l$ AND NO-LOAD FLOW Q_{nl} FOR VARIOUS 0-TO-PK VOLTAGE LEVELS. PUMPS ARE IDENTIFIED BY THE NOTATION IN Tab. 3, AND THE NUMBERS IN BRACKETS CORRESPOND TO THE DESIGN SPACE COORDINATES $[t_p, w_v]$. THE APPLIED VOLTAGE OF 24V WAS USED TO COMPARE MEASURED AND CALCULATED PERFORMANCE UNDER THE SAME CONDITIONS. THE FOUR BOXED VALUES INDICATE THE HIGHEST MEASURED AND CALCULATED PRESSURE AND FLOW VALUES AT THAT SAME VOLTAGE.

applied	P_{bl}		Q_{nl}		applied	P_{bl}		Q_{nl}		applied	P_{bl}		Q_{nl}	
voltage	meas	calc	meas	calc	voltage	meas	calc	meas	calc	voltage	meas	calc	meas	calc
V	kPa		ml/min		V	kPa		ml/min		V	kPa		ml/min	
	P1 [76,150]					P2 [76,300]					P3 [76,600]			
16		1.35					2.24					1.91		
32		4.65					5.44					1.91		
64	2.3	11.3	1.1	9.5	64	0.89	6.27	1.7	20	64	0	1.91	0	23
125		48.7			125	4.6	6.27			125	0.14	1.91		
	P4 [102,150]					P5 [102,300]					P6 [102,600]			
16		1.72					2.63					1.69		
32		5.50					5.42					1.69		
64	4.5	13.3	1.4	11	64	1.3	5.42	1.8	16	64	0	1.69	0	19
125	***13***	***24.1***			125	9.6	5.42			100	0.068	1.69		
	P7 [178,150]					P8 [178,300]					P9 [176,600]			
16		2.58					3.57					1.16		
32		7.59					3.87					1.16		
64	4.3	12.7	1.4	7.7	64	0.55	3.87	0.78	10	64	0	1.16	0	11
125	12	12.7			125		3.87			125		1.16		

was reached at a lower voltage since the valve resistance was lower than actual. Again, it appears that proper handling of the additional loss effects of flow entering and leaving the valves is necessary.

It can further be said regarding P_{bl} that the model correctly predicted the pump that produced the highest measured value at the 64 v level, which was pump P4. In addition, the same pump produced the highest pressure overall, generating 13 kPa at 125 V (approximately 2 psi). This value of pressure is higher than we have been able to report for these materials and pump size [15,16], although unpublished values of approximately 6 psi have been observed in our laboratory for smaller silicon/Pyrex pumps [18]. Lastly, the model agreed well with measurement in that pressure generated dropped precipitously with increasing valve size as seen by comparing pumps in any row of Tab. 4. This along with the prediction of the highest pressure pump may be the most important results of the study, since they indicate that the model is able to predict the best configuration in terms of pressure performance even though the quantitative value of pressure is over-estimated.

Turning to net flow capability, pump P5 produced the maximum measured Q_{nl}, but the model only agreed with measured trends in that reducing valve size or increasing membrane thickness relative to that pump resulted in reduced flow (c.f. pumps P4 and P8, respectively). The main failing of the model was prediction of increasing no-load flow with increasing valve size without obvious limits in the design space as seen in Fig. 6, whereas in all rows of Tab. 4 experimentally measured flow rate dropped precipitously at the largest valve size. This might be explained by noting the model of the no-load condition is not necessarily realistic. The no-load condition means that with no back pressure, the only hindrance to net flow is viscous loss as fluid oscillates back an forth in the valves. And as the valve size increases, increased peak flow rate may not be accompanied by a increased flow loss if wall shear forces in the larger valve do not increase sufficiently. Thus, as long as there is absolutely no back pressure, the flow rate may continue to grow. However, in Fig. 8 a decrease in no-load flow with increasing valve size can be detected since each near-vertical row of data points corresponds to a particular membrane thickness with valve size increasing moving downward. Each the column moves slightly toward decreasing Q_{nl} at their lower end. However, this modeling limitation may not be

important since for any practical application, a pump is not going to be utilized in a no-load condition. An improved model could be based on a load resistor and capacitor in parallel, where an attempt could be made to determine values for each parameter that would more closely model a "low-load" flow. This could be a substantial modeling improvement since experimental values of pump performance for fixed-geometry pumps characteristically lie along a straight line between experimentally determined P_{bl} and Q_{nl} on a pressure versus flow rate plot [18].

In conclusion, the goal of this study was achieved in that the inclusion of a non-linear sub-model to calculate net block load pressure and no-load flow into an existing linear model represented an improvement in predicting the performance of actual pumps compared to previous more indirect design methods. Prediction of design parameters that lead to best pressure performance was successful even though the estimated pressures over-estimated actual values. The results suggest that inclusion of valve entry and exit losses, should lead to better predictive power.

ACKNOWLEDGMENTS

This work was supported in part by a donation for research in microfluidics from Motorola Labs, Tempe, AZ and a Design News/ANSYS College Student Design Engineering Award. Travis Walter, who was an undergraduate student during part of the project, contributed greatly to the experimental portion of the work.

REFERENCES

[1] Tesla, N., 1920. Valvular conduit. U.S. Patent No. 1,329,559.

[2] Reed, J. L., 1993. Fluidic rectifier. U. S. Patent No. 5,265,636, Nov. 30.

[3] Stemme, E., and Stemme, G., 1993. "A valveless diffuser/nozzle-based fluid pump". *Sens. and Actuators Series A,* **A39**(2), pp. 159–167.

[4] Gravesen, P., Branebjerg, J., and Sondergard, J., 1993. "Microfluidics—a review". *Journal of Micromechanics and Microengineering,* **3**, pp. 168–182.

[5] Forster, F., Bardell, R., Afromowitz, M., and Sharma, N., 1995. "Design, fabrication and testing of fixed-valve micropumps". In Proceedings of the ASME Fluids Engineering Division 1995 (San Francisco), D. C. Wiggert et al., eds., Vol. FED–234, ASME, pp. 39–44.

[6] Gerlach, T., Schuenemann, M., and Wurmus, H., 1995. "A new micropump principle of the reciprocating type using pyramidic micro flowchannels as passive valves". *Journal of Micromechanics and Microengineering,* **5**, pp. 199–201.

[7] Olsson, A., Enoksson, P., Stemme, G., and Stemme, E., 1995. "A valve-less planar pump in silicon". In Transducers '95 (Stockholm), Vol. 2, IEEE, pp. 291–294.

[8] Laser, D. J., and Santiago, J. G., 2004. "A review of micropumps". *Journal of Micromechanics and Microengineering,* **14**, pp. R35–R64.

[9] Morris, C. J., and Forster, F. K., 2000. "Optimization of a circular piezoelectric bimorph for a micropump driver". *Journal of Micromechanics and Microengineering,* **10**(3), pp. 459–465.

[10] Morris, C. J., and Forster, F. K., 2003. "Low-order modeling of resonance for fixed-valve micropumps based on first principles". *Journal of Microelectromechanical Systems,* **12**(3), pp. 325–334.

[11] Morris, C. J., and Forster, F. K., 2004. "Oscillatory flow in microchannels: comparison of exact and approximate imdedance models with experiment". *Experiments in Fluids,* **36**(6), pp. 928–937.

[12] Forster, F. K., and Williams, B. E., 2002. "Parametric design of fixed-geometry microvalves—the Tesser valve". In Proceedings of the ASME Fluids Engineering Division, International Mechanical Engineering Congress and Exposition (New Orleans), A. Ogut, ed., Vol. FED-258, ASME, pp. 431–437.

[13] Gamboa, A. R., and Forster, F. K., 2004. "Is there a best fixed-geometry valve for micropumps?". In Proceedings of the ASME Fluids Engineering Division 2004 (Anaheim).

[14] Gamboa, A. R., Morris, C. J., and Forster, F. K., 2005. "Improvements in fixed-valve micropump performance through shape optimization of valves". *Journal of Fluids Engineering,* **FED–127**(March), pp. 339–346.

[15] Morris, C. J., Chung, J. Y., Rahm, P. E., Forster, F. K., Shekarriz, R., and Faulkner, D., 2004. "Electronic cooling systems based on fixed-valve micropump networks". In Solid-State Sensor, Actuator and Microsystems Workshop, Transducers Research Foundation, Inc., pp. 152–155.

[16] Faulkner, D., Ward, C., Gilbuena, D., Shekarriz, R., and Forster, F. K., 2006. "Fixed valve piezoelectric micropump for miniature thermal management module". In Proceedings of the ASME Fluids Engineering Division Summer Meeting and Exhibition (Miami).

[17] Gamboa, A. R., 2004. "Shape optimization of the nozzle-diffuser and tesla-type valves for applications in micropumps". M. S. Thesis, University of Washington, Seattle.

[18] Morris, C. J., 2000. "Parameter determination for low-order models of a fixed-valve micropump". M. S. Thesis, University of Washington, Seattle.